Journal of Computational Physics 229 (2010) 1150–1166

Contents lists available at ScienceDirect

Journal of Computational Physics

journal homepage: www.elsevier.com/locate/jcp

The monotonic Quartic Spline Method (QSM) for conservative transport problems ☆

M. Zerroukat *, A. Staniforth, N. Wood

Met Office, FitzRoy Road, Exeter EX1 3PB, United Kingdom

ARTICLE INFO

Article history:
Received 15 April 2009
Received in revised form 1 October 2009
Accepted 10 October 2009
Available online 28 October 2009

PACS:
02.60.Lj
02.70.Bf
47.11.Df
92.30.Ef

Keywords:
Advection
Conservation
Monotonicity
PPM
PSM
Remapping

ABSTRACT

A quartic spline based remapping algorithm is developed and illustrative tests of it are presented herein. To ensure mass conservation, the scheme solves an integral form of the transport equation rather than the differential form. The integrals are computed from reconstructed quartic splines with mass conservation constraints. For higher dimensions, this remapping can be used within a standard directional splitting methodology or within the flow-dependent cascade splitting approach. A high-order grid and sub-grid based monotonic filter is also incorporated into the overall scheme. This filter is independent of the underlying spline representation adopted here, and is of more general application.

1. Introduction

Remapping algorithms, such as the widely used Piecewise Parabolic Method (PPM) [1], are an important component in many advection schemes for conservative transport. These remappings are also the building blocks of many of the inherently conserving semi-Lagrangian schemes [2–11].

An alternative to PPM, based on the Parabolic Spline Method (PSM), was presented in [12] and demonstrated in [13] for two-dimensional conservative transport in Cartesian and spherical geometries. PSM is similar to PPM, but more accurate (due to its "best approximation" property), whilst being 60% more efficient [12]. PSM also incorporates a more selective, and less damping, monotonic filter than that used in the original PPM [1]. PSM achieves monotonicity without (except in extreme cases) reducing the order of the piecewise polynomial, and it well captures steep gradients and curvature without recourse to artificial steepening.

The goal of the present paper is to generalise the PSM remapping algorithm to higher order, for increased accuracy. Being based on a quartic spline, the resulting algorithm is termed the Quartic Spline Method (QSM). Similarly to PSM, QSM also has

☆ © British Crown copyright.

* Corresponding author.
E-mail address: Mohamed.Zerroukat@metoffice.gov.uk (M. Zerroukat).
URL: http://www.metoffice.gov.uk (M. Zerroukat).

0021-9991/$ - see front matter Crown Copyright © 2009 Published by Elsevier Inc. All rights reserved.
doi:10.1016/j.jcp.2009.10.018

a "best approximation" property: whereas PSM is optimal within the class of *second*-order polynomial representations of density, QSM is optimal within the class of *fourth*-order ones.

The rest of the paper is organised as follows: Section 2 details the QSM remapping algorithm and its properties; its monotonic filter is described in Section 3; results using the proposed scheme are presented in Section 4 and compared with those using PSM; and conclusions are summarised in Section 5.

2. The Quartic Spline Method (QSM)

2.1. Problem definition

Consider passive 1D conservative transport of a scalar quantity ρ governed, in the absence of sources and sinks, by

$$\frac{\partial \rho}{\partial t} + \frac{\partial}{\partial x}(u\rho) = 0, \tag{1}$$

where $\rho(x,t)$ is the density (amount of scalar per unit length) of the transported quantity, and $u(x,t)$ is the transporting velocity field. Assume a finite fluid volume bounded by two arbitrary boundaries $x_1 = x_1(x,t)$ and $x_2 = x_2(x,t)$ moving with the fluid, so that

$$\frac{dx_1}{dt} = u(x_1,t), \quad \frac{dx_2}{dt} = u(x_2,t). \tag{2}$$

Integrating (1) with respect to x between two arbitrary moving boundaries $x_L = x_L(x,t)$ and $x_R = x_R(x,t)$, and making use of Leibniz' rule, then leads [5] to the classical integral form of the tracer conservation equation

$$\frac{d\mathfrak{M}(x_L,x_R,t)}{dt} \equiv \frac{d}{dt}\left(\int_{x_L(t)}^{x_R(t)} \rho(x,t)dx\right) = 0. \tag{3}$$

Eq. (3) simply states that the mass $\mathfrak{M}(x_L,x_R,t)$ contained between any two boundaries, $x_L(t)$ and $x_R(t)$, that move with the fluid, is invariant in time, i.e. $\mathfrak{M}$ is conserved.

Since $x_L(t)$ and $x_R(t)$ in (3) are any two points travelling with the fluid, one can consider that these moving boundaries instantaneously coincide at time t^{n+1} with the boundaries of an Eulerian Control Volume (ECV). Their upstream positions $x_L(t^n)$ and $x_R(t^n)$ at time t^n then form the left and right boundaries of the associated upstream Lagrangian Control Volume (LCV). In other words, since the fluid is a continuum, then the fluid contained in the Lagrangian segment $[x_L^d, x_R^d] \equiv [x_L(t^n), x_R(t^n)]$ is completely transported to the Eulerian segment $[x_L(t^{n+1}), x_R(t^{n+1})]$ (this provides the basis of the SLICE scheme [2]).

To discretise (3), consider the general case where the computational 1D domain $\Omega = [x_{min}, x_{max}]$ is subdivided into N ECV's with (possibly unequal) spacing $h_i \equiv x_{i+1/2} - x_{i-1/2}$ $(i = 1,2,\ldots,N)$, where $x_{i-1/2}$ and $x_{i+1/2}$ are respectively the left and right boundaries of ECV_i. For a closed domain, the left boundary is at $x = x_{1/2}$ and the right boundary at $x = x_{N+1/2}$. For a periodic domain, $x_{N+i+1/2} \equiv x_{i-1/2}$ $(i = 0, \pm1, \pm2, \ldots)$.

Defining the gridbox-averaged density at time t as

$$\bar{\rho}_i(t) \equiv \frac{1}{h_i}\int_{x_{i-1/2}}^{x_{i+1/2}} \rho(x,t)dx \equiv \frac{1}{h_i}\mathfrak{M}(x_{i-1/2}, x_{i+1/2}, t) \equiv \frac{1}{h_i}\mathfrak{M}_i, \tag{4}$$

the time-discretisation of (3) can then be rewritten as

$$\bar{\rho}_i^{n+1} \equiv \bar{\rho}_i(t^{n+1}) \equiv \frac{1}{h_i}(\mathfrak{M}_i)^{n+1} = \frac{1}{h_i}\left(\mathfrak{M}_i^d\right)^n, \tag{5}$$

where

$$\mathfrak{M}_i^d \equiv \int_{x_{i-1/2}^d}^{x_{i+1/2}^d} \rho(x,t)dx. \tag{6}$$

Here superscript n denotes evaluation at time t^n, superscript d denotes association with a departure-point value (as in semi-Lagrangian schemes [14]), and $x_{i-1/2}^d$ and $x_{i+1/2}^d$ are respectively the left- and right-hand boundaries of LCV_i at time t^n, determined from numerical integration of (2) – see e.g. [14].

In general, the shape of $\rho(x,t^n)$ is not known *a priori*, and hence (6) cannot be evaluated. Instead piecewise polynomials that use the given discrete gridbox-averaged values can be reconstructed. Previous approaches have used either piecewise constant, piecewise linear [15], piecewise parabolic [1,12] or piecewise cubic [2,8] polynomials. Herein a Quartic Spline Method is proposed.

2.2. Formulation

A quartic spline is the union of piecewise-defined quartic polynomials, constructed so the resulting composite function, together with its first, second, and third derivatives, are all continuous everywhere within the domain. In the present context, the quartic spline may be written as

$$\rho(x) = \sum_{i=1}^{N} \rho_i(x), \tag{7}$$

where $\rho_i(x)$ is a quartic polynomial defined on the interval $\left[x_{i-\frac{1}{2}}, x_{i+\frac{1}{2}}\right]$. The quartic polynomial $\rho_i(x)$ may be uniquely written in terms of the five meshpoint values $\rho_{i-\frac{1}{2}} \equiv \rho\left(x_{i-\frac{1}{2}}\right)$, $\rho_{i+\frac{1}{2}} \equiv \rho\left(x_{i+\frac{1}{2}}\right)$, $M_{i-\frac{1}{2}} \equiv .(d^3\rho/dx^3)|_{x_{i-\frac{1}{2}}}$, $M_{i+\frac{1}{2}} \equiv (d^3\rho/dx^3)|_{x_{i+\frac{1}{2}}}$ and $\bar{\rho}_i \equiv \int_{x_{i-\frac{1}{2}}}^{x_{i+\frac{1}{2}}} \rho_i(x)dx/h_i$. [Note: of these five values, only $\bar{\rho}_i$ is given, and the remaining four remain to be determined via imposition of continuity constraints.] Thus

$$\rho_i(\xi) = a_i^{(0)} + a_i^{(1)}\xi + a_i^{(2)}\xi^2 + a_i^{(3)}\xi^3 + a_i^{(4)}\xi^4, \quad \xi \in [0,1], \tag{8}$$

where

$$\xi \equiv \left(\frac{x - x_{i-\frac{1}{2}}}{h_i}\right) \tag{9}$$

is a dimensionless local coordinate, and $\left(a_i^{(0)}, a_i^{(1)}, a_i^{(2)}, a_i^{(3)}, a_i^{(4)}\right)$ are coefficients defined such that

$$a_i^{(0)} = \rho_{i-\frac{1}{2}}, \tag{10}$$

$$a_i^{(1)} = -2\rho_{i+\frac{1}{2}} - 4\rho_{i-\frac{1}{2}} + \frac{h_i^3}{20}M_{i-\frac{1}{2}} + \frac{h_i^3}{30}M_{i+\frac{1}{2}} + 6\bar{\rho}_i, \tag{11}$$

$$a_i^{(2)} = 3\rho_{i+\frac{1}{2}} + 3\rho_{i-\frac{1}{2}} - \frac{7h_i^3}{40}M_{i-\frac{1}{2}} - \frac{3h_i^3}{40}M_{i+\frac{1}{2}} - 6\bar{\rho}_i, \tag{12}$$

$$a_i^{(3)} = \frac{h_i^3}{6}M_{i-\frac{1}{2}}, \tag{13}$$

$$a_i^{(4)} = \frac{h_i^3}{24}M_{i+\frac{1}{2}} - \frac{h_i^3}{24}M_{i-\frac{1}{2}}, \tag{14}$$

$$\bar{\rho}_i = \int_0^1 \rho_i(\xi)d\xi. \tag{15}$$

Successively differentiating (8) then gives

$$\frac{d\rho_i(\xi)}{d\xi} = a_i^{(1)} + 2a_i^{(2)}\xi + 3a_i^{(3)}\xi^2 + 4a_i^{(4)}\xi^3, \tag{16}$$

$$\frac{d^2\rho_i(\xi)}{d\xi^2} = 2a_i^{(2)} + 6a_i^{(3)}\xi + 12a_i^{(4)}\xi^2, \tag{17}$$

$$\frac{d^3\rho_i(\xi)}{d\xi^3} = 6a_i^{(3)} + 24a_i^{(4)}\xi, \tag{18}$$

$$\frac{d^4\rho_i(\xi)}{d\xi^4} = 24a_i^{(4)}. \tag{19}$$

By construction, $\rho(x)$, as defined by (7)–(19), is continuous and has continuous third derivatives at all meshpoints $x_{i\pm\frac{1}{2}}$, $i = 1, 2, \ldots, N$. Imposing the conditions that its first and second derivatives also be continuous at these same meshpoints then fully defines the quartic spline (apart from boundary considerations – see Section 2.3) and yields two equations that relate the five quantities $\rho_{i-\frac{1}{2}}$, $\rho_{i+\frac{1}{2}}$, $M_{i-\frac{1}{2}}$, $M_{i+\frac{1}{2}}$ and $\bar{\rho}_i$. This is achieved for first derivatives by equating $(d\rho_i/dx)|_{x_{i+\frac{1}{2}}}$ and $(d\rho_{i+1}/dx)|_{x_{i+\frac{1}{2}}}$, both evaluated using (16). Thus

$$\frac{h_i^2}{30}M_{i-\frac{1}{2}} - \frac{1}{20}\left(h_{i+1}^2 - h_i^2\right)M_{i+\frac{1}{2}} - \frac{h_{i+1}^2}{30}M_{i+\frac{3}{2}} + \frac{2}{h_i}\rho_{i-\frac{1}{2}} + \left(\frac{4}{h_i} + \frac{4}{h_{i+1}}\right)\rho_{i+\frac{1}{2}} + \frac{2}{h_{i+1}}\rho_{i+\frac{3}{2}} = \frac{6}{h_{i+1}}\bar{\rho}_{i+1} + \frac{6}{h_i}\bar{\rho}_i. \tag{20}$$

Similarly, for second derivatives, i.e. equating $(d^2\rho_i/dx^2)|_{x_{i+\frac{1}{2}}}$ and $(d^2\rho_{i+1}/dx^2)|_{x_{i+\frac{1}{2}}}$, one obtains

$$\frac{1}{20}\left[3h_iM_{i-\frac{1}{2}} + 7(h_i + h_{i+1})M_{i+\frac{1}{2}} + 3h_{i+1}M_{i+\frac{3}{2}}\right] - 6\left[\frac{1}{h_{i+1}^2}\rho_{i+\frac{3}{2}} + \left(\frac{1}{h_{i+1}^2} - \frac{1}{h_i^2}\right)\rho_{i+\frac{1}{2}} - \frac{1}{h_i^2}\rho_{i-\frac{1}{2}}\right] = -12\left(\frac{1}{h_{i+1}^2}\bar{\rho}_{i+1} - \frac{1}{h_i^2}\bar{\rho}_i\right). \tag{21}$$

The quantities on the right-hand sides of (20) and (21) are all known, whereas those on the left-hand sides are not. Eqs. (20) and (21) couple the unknown M's to the unknown ρ's. To obtain an efficient solution algorithm, the following steps are followed to decouple the equations:

1. Supplement (20) and (21) by their index increments (i.e. $i \to i+1$ everywhere in (20) and (21)) and index decrements (i.e. $i \to i-1$ everywhere in (20) and (21)). This gives a set of six linear equations that relate the ten unknown quantities $M_{i-\frac{3}{2}}$, $M_{i-\frac{1}{2}}$, $M_{i+\frac{1}{2}}$, $M_{i+\frac{3}{2}}$, $M_{i+\frac{5}{2}}$, $\rho_{i-\frac{3}{2}}$, $\rho_{i-\frac{1}{2}}$, $\rho_{i+\frac{1}{2}}$, $\rho_{i+\frac{3}{2}}$ and $\rho_{i+\frac{5}{2}}$, to the four known quantities $\bar{\rho}_{i-1}$, $\bar{\rho}_i$, $\bar{\rho}_{i+1}$ and $\bar{\rho}_{i+2}$.
2. Eliminate $\rho_{i-\frac{3}{2}}$, $\rho_{i-\frac{1}{2}}$, $\rho_{i+\frac{3}{2}}$ and $\rho_{i+\frac{5}{2}}$ from this set of six equations to reduce it to two equations for the six unknown quantities $M_{i-\frac{3}{2}}$, $M_{i-\frac{1}{2}}$, $M_{i+\frac{1}{2}}$, $M_{i+\frac{3}{2}}$, $M_{i+\frac{5}{2}}$ and $\rho_{i+\frac{1}{2}}$.
3. Eliminate $\rho_{i+\frac{1}{2}}$ from these two equations to obtain an equation for the five unknown quantities $M_{i-\frac{3}{2}}$, $M_{i-\frac{1}{2}}$, $M_{i+\frac{1}{2}}$, $M_{i+\frac{3}{2}}$ and $M_{i+\frac{5}{2}}$. This leads to a pentadiagonal set of linear equations. With appropriate boundary conditions (see Section 2.3) this pentadiagonal set can be solved for $M_{i-\frac{3}{2}}$, $M_{i-\frac{1}{2}}$, $M_{i+\frac{1}{2}}$, $M_{i+\frac{3}{2}}$ and $M_{i+\frac{5}{2}}$.
4. The remaining quantity, $\rho_{i+\frac{1}{2}}$, is then obtained from the now-known quantities $M_{i-\frac{3}{2}}$, $M_{i-\frac{1}{2}}$, $M_{i+\frac{1}{2}}$, $M_{i+\frac{3}{2}}$ and $M_{i+\frac{5}{2}}$ using the remaining equation of the two equations of step 2.

For simplicity, consider first uniform resolution in a periodic domain. Eqs. (20) and (21) then reduce to

$$-\frac{h^2}{30}\left(M_{i+\frac{3}{2}} - M_{i-\frac{1}{2}}\right) + \frac{2}{h}\left(\rho_{i-\frac{1}{2}} + 4\rho_{i+\frac{1}{2}} + \rho_{i+\frac{3}{2}}\right) = \frac{6}{h}(\bar{\rho}_{i+1} + \bar{\rho}_i), \tag{22}$$

$$\frac{h}{20}\left(3M_{i-\frac{1}{2}} + 14M_{i+\frac{1}{2}} + 3M_{i+\frac{3}{2}}\right) - \frac{6}{h^2}\left(\rho_{i+\frac{3}{2}} - \rho_{i-\frac{1}{2}}\right) = -\frac{12}{h^2}(\bar{\rho}_{i+1} - \bar{\rho}_i). \tag{23}$$

Using (22) and (23), and following the steps outlined above, leads to the pentadiagonal system of equations

$$\frac{1}{120}\left(M_{i-\frac{3}{2}} + 26M_{i-\frac{1}{2}} + 66M_{i+\frac{1}{2}} + 26M_{i+\frac{3}{2}} + M_{i+\frac{5}{2}}\right) = \frac{1}{h^3}(\bar{\rho}_{i+2} - 3\bar{\rho}_{i+1} + 3\bar{\rho}_i - \bar{\rho}_{i-1}), \tag{24}$$

and to the diagnostic equation

$$\rho_{i+\frac{1}{2}} = \frac{1}{12}(-\bar{\rho}_{i-1} + 7\bar{\rho}_i + 7\bar{\rho}_{i+1} - \bar{\rho}_{i+2}) - \frac{h^3}{1440}\left(M_{i-\frac{3}{2}} + 22M_{i-\frac{1}{2}} - 22M_{i+\frac{3}{2}} - M_{i+\frac{5}{2}}\right), \tag{25}$$

for $\rho_{i+\frac{1}{2}}$.

The counterparts of (24) and (25) for non-uniform resolution are more complicated, and are given in Appendix A.

2.3. Boundary conditions

For a periodic domain, there are exactly the right number of discrete equations to determine $M_{i+1/2}$ and $\rho_{i+1/2}$ from (24) and (25) at all points $x_{i+1/2}$ in the domain. However, for a closed domain, with boundaries located at $x = x_{1/2}$ and $x = x_{N+1/2}$, an extra two equations (i.e. boundary conditions) are needed at each boundary to close the discrete equation set [16]: (24) and (25) cannot be applied at the two boundaries, nor at the first interior points, since points outside the domain are referenced.

To address this issue, whilst simultaneously ensuring smoothness of the resulting spline, assume instead the "natural" boundary conditions $d^2\rho/dx^2 = d^3\rho/dx^3 = 0$ at the left and right boundaries (see [16] and the discussion in Section 2.6), i.e.

$$\left(\frac{d^2\rho}{dx^2}\right)\Big|_{x_{\frac{1}{2}}} = \left(\frac{d^3\rho}{dx^3}\right)\Big|_{x_{\frac{1}{2}}} = \left(\frac{d^2\rho}{dx^2}\right)\Big|_{x_{N+\frac{1}{2}}} = \left(\frac{d^3\rho}{dx^3}\right)\Big|_{x_{N+\frac{1}{2}}} = 0. \tag{26}$$

Applying (26), and following the procedure of Section 2.2 that led to (21), then gives

$$M_{\frac{1}{2}} = 0, \quad \rho_{\frac{1}{2}} + \rho_{\frac{3}{2}} - \frac{h_1^3}{40}M_{\frac{3}{2}} = 2\bar{\rho}_1, \quad M_{N+\frac{1}{2}} = 0, \quad \rho_{N-\frac{1}{2}} + \rho_{N+\frac{1}{2}} + \frac{h_N^3}{40}M_{N-\frac{1}{2}} = 2\bar{\rho}_N. \tag{27}$$

To obtain an efficient solution algorithm, the following steps are followed to decouple the equations at the left boundary (with a similar procedure for the right boundary):

1. Supplement the first two equations of (27) with the continuity constraints (20) and (21), both evaluated for $i = 1$ and $i = 2$, to obtain a set of six equations that relate $M_{\frac{1}{2}}$, $M_{\frac{3}{2}}$, $M_{\frac{5}{2}}$, $M_{\frac{7}{2}}$, $\rho_{\frac{1}{2}}$, $\rho_{\frac{3}{2}}$, $\rho_{\frac{5}{2}}$ and $\rho_{\frac{7}{2}}$ to the known quantities $\bar{\rho}_1$, $\bar{\rho}_2$ and $\bar{\rho}_3$.
2. Eliminate $M_{\frac{1}{2}}$, $\rho_{\frac{1}{2}}$, $\rho_{\frac{3}{2}}$, $\rho_{\frac{5}{2}}$ and $\rho_{\frac{7}{2}}$ from this set of six equations to obtain an equation for the unknown quantities $M_{\frac{3}{2}}$, $M_{\frac{5}{2}}$ and $M_{\frac{7}{2}}$ in terms of the known quantities $\bar{\rho}_1$, $\bar{\rho}_2$ and $\bar{\rho}_3$.
3. Further manipulate this set of six equations to obtain $\rho_{\frac{1}{2}}$ and $\rho_{\frac{3}{2}}$ in terms of $M_{\frac{3}{2}}$, $M_{\frac{5}{2}}$ and $M_{\frac{7}{2}}$.

For uniform resolution these steps lead to

$$M_{\frac{1}{2}} = 0, \tag{28}$$

$$\frac{h^3}{120}\left(93M_{\frac{3}{2}} + 27M_{\frac{5}{2}} + M_{\frac{7}{2}}\right) = \bar{\rho}_1 - 2\bar{\rho}_2 + \bar{\rho}_3, \tag{29}$$

$$\frac{1}{120}\left(M_{i-\frac{3}{2}} + 26M_{i-\frac{1}{2}} + 66M_{i+\frac{1}{2}} + 26M_{i+\frac{3}{2}} + M_{i+\frac{5}{2}}\right) = \frac{1}{h^3}(\bar{\rho}_{i+2} - 3\bar{\rho}_{i+1} + 3\bar{\rho}_i - \bar{\rho}_{i-1}), \quad i = 2,3,\ldots,N-2, \tag{30}$$

$$\frac{h^3}{120}\left(M_{N-\frac{5}{2}} + 27M_{N-\frac{3}{2}} + 93M_{N-\frac{1}{2}}\right) = -(\bar{\rho}_{N-2} - 2\bar{\rho}_{N-1} + \bar{\rho}_N), \tag{31}$$

$$M_{N+\frac{1}{2}} = 0, \tag{32}$$

$$\rho_{\frac{1}{2}} = \frac{1}{2}(3\bar{\rho}_1 - \bar{\rho}_2) + \frac{h^3}{240}\left(26M_{\frac{3}{2}} + M_{\frac{5}{2}}\right), \tag{33}$$

$$\rho_{\frac{3}{2}} = \frac{1}{2}(\bar{\rho}_1 + \bar{\rho}_2) - \frac{h^3}{240}\left(20M_{\frac{3}{2}} + M_{\frac{5}{2}}\right), \tag{34}$$

$$\rho_{i+\frac{1}{2}} = \frac{1}{12}(-\bar{\rho}_{i-1} + 7\bar{\rho}_i + 7\bar{\rho}_{i+1} - \bar{\rho}_{i+2}) - \frac{h^3}{1440}\left(M_{i-\frac{3}{2}} + 22M_{i-\frac{1}{2}} - 22M_{i+\frac{3}{2}} - M_{i+\frac{5}{2}}\right), \quad i = 2,3,\ldots,N-2, \tag{35}$$

$$\rho_{N-\frac{1}{2}} = \frac{1}{2}(\bar{\rho}_{N-1} + \bar{\rho}_N) + \frac{h^3}{240}\left(M_{N-\frac{3}{2}} + 20M_{N-\frac{1}{2}}\right), \tag{36}$$

$$\rho_{N+\frac{1}{2}} = \frac{1}{2}(3\bar{\rho}_N - \bar{\rho}_{N-1}) - \frac{h^3}{240}\left(M_{N-\frac{3}{2}} + 26M_{N-\frac{1}{2}}\right), \tag{37}$$

where (24) and (25) have been inserted into the above equations to complete the two equation sets to determine $M_{\frac{1}{2}}, M_{\frac{3}{2}}, \ldots, M_{N+\frac{1}{2}}$ and $\rho_{\frac{1}{2}}, \rho_{\frac{3}{2}}, \ldots, \rho_{N+\frac{1}{2}}$.

The counterparts of (28)–(37) for non-uniform resolution are more complicated, and are given in Appendix A.

The pentadiagonal matrix associated with (28)–(31) has non-zero determinant, and is therefore invertible. The equation set (28)–(32) is solved for $M_{\frac{1}{2}}, M_{\frac{3}{2}}, \ldots, M_{N+\frac{1}{2}}$ using the band-diagonal solver given in Section 2.4 of [17]. Eqs. (33)–(37) are then used to obtain $\rho_{\frac{1}{2}}$, $\rho_{\frac{3}{2}}$, $\rho_{N-\frac{1}{2}}$, $\rho_{N+\frac{1}{2}}$. This, via the use of (10)–(14), results in all of the coefficients in the piecewise quartic spline (8) representation now being known.

2.4. Computation of piecewise integrals

Having defined the piecewise-defined functions $\rho_i(x)$ for each ECV_i, the mass $\left(\mathfrak{M}_i^d\right)^n$, given by (6), of LCV_i, which extends over the segment $\left[x_{i-1/2}^d, x_{i+1/2}^d\right]$ at time t^n, is computed as

$$\left(\mathfrak{M}_i^d\right)^n = \begin{cases} h_l \int_{\xi_{i-1/2}^d}^{1} \rho_l^n(\xi)d\xi + \sum_{j=l+1}^{m-1} h_j\bar{\rho}_j^n + h_m \int_0^{\xi_{i+1/2}^d} \rho_m^n(\xi)d\xi, & m \geqslant l+1, \\ h_l \int_{\xi_{i-1/2}^d}^{\xi_{i+1/2}^d} \rho_l^n(\xi)d\xi, & m = l, \end{cases} \tag{38}$$

where l and $m \geqslant l$ are the ECV indices associated with the segments in which $x_{i-1/2}^d$ and $x_{i+1/2}^d$ lie, i.e. $x_{i-1/2}^d \in [x_{l-1/2}, x_{l+1/2}]$ and $x_{i+1/2}^d \in [x_{m-1/2}, x_{m+1/2}]$. Also $\xi_{i\pm1/2}^d$ are the local coordinates corresponding to $x_{i\pm1/2}^d$, i.e. $\xi_{i-1/2}^d = (x_{i-1/2}^d - x_{l-1/2})/h_l$ and $\xi_{i+1/2}^d = (x_{i+1/2}^d - x_{m-1/2})/h_m$. The integrals on the right-hand side of (38) are evaluated analytically.

2.5. Higher dimensions

For higher dimensions, the present 1D remapping algorithm can be used within a standard directional splitting methodology or within the flow-dependent cascade methodology used in SLICE [2,3]. In both approaches, a 2D (or 3D) problem is spatially split into sets of 1D remapping problems to be solved using an algorithm such as PSM or PPM.

2.6. Link with classical quintic splines and the best approximation property

To link the quartic spline developed above to classical quintic splines, first define a new variable, cumulative mass, by

$$R(x) \equiv R_{1/2} + \int_{x_{1/2}}^{x} \rho(x)dx, \tag{39}$$

where $R_{1/2}$ is an arbitrary non-negative constant. Differentiating (39) gives

$$\frac{dR(x)}{dx} = \rho(x), \tag{40}$$

which, after integration from $x = x_{i-1/2}$ to $x = x_{i+1/2}$ and use of (15), then yields

$$\frac{1}{h_i}\left(R_{i+\frac{1}{2}} - R_{i-\frac{1}{2}}\right) = \frac{1}{h_i}\int_{x_{i-1/2}}^{x_{i+1/2}} \rho(x)dx \equiv \bar{\rho}_i. \tag{41}$$

Eq. (24) can now be rewritten using (41) as

$$\frac{1}{120}\left(M_{i-\frac{3}{2}} + 26M_{i-\frac{1}{2}} + 66M_{i+\frac{1}{2}} + 26M_{i+\frac{3}{2}} + M_{i+\frac{5}{2}}\right) = \frac{1}{h^4}\left(R_{i+\frac{5}{2}} - 4R_{i+\frac{3}{2}} + 6R_{i+\frac{1}{2}} - 4R_{i-\frac{1}{2}} + R_{i-\frac{3}{2}}\right). \tag{42}$$

Comparing this result for uniform resolution with (4.2.13) of [16], and taking account of differences in notation ($R \to S$) and indexing convention (all indices of R are incremented by 1/2), it is seen that they are formally equivalent. Similarly, the non-uniform resolution counterpart (59) to (42) is equivalent to the first equation on p. 122 of [16]. Also, the (non-uniform resolution) constraint Eqs. (20) and (21) for continuity at gridpoints of $d\rho/dx$ and $d^2\rho/dx^2$, respectively, are seen to be equivalent to Eqs. (4.1.31) and (4.1.30), respectively, of [16] for continuity of d^2R/dx^2 and d^3R/dx^3.

The quartic spline defined herein in terms of the discrete values $\bar{\rho}_i$ is therefore equivalent to a classical quintic spline defined in terms of the discrete values $R_{i+1/2}$ of a cumulative mass function: both satisfy identical continuity constraints after taking into consideration that one (ρ) is the derivative of the other (R), and that a quintic spline is uniquely defined [16]. In other words, the values of $\rho_{i+1/2}$ obtained from (25) are the same as would result from fitting a classical quintic spline through the discrete values $R_{i+1/2}$ of the cumulative mass function (39) and evaluating dR/dx at gridpoints $x_{i+1/2}$. The values of $R_{i+1/2}$, if needed, can be recursively materialised from (41) by imposing the arbitrary reference value $R_{1/2} = 0$ (the $R_{i+1/2}$'s are only defined to within an arbitrary additive constant).

A property of classical quintic splines ([16], Section 5.4) is the"minimum norm" property: of all interpolating piecewise-quintic functions, the quintic spline minimises the norm $\int(d^3R/dx^3)^2dx$. Since, from (40), $dR/dx = \rho$, this means that $\int(d^2\rho/dx^2)^2dx$ is minimised over the domain, i.e. the mean-squared curvature of ρ is minimised.

From (40), ρ is the derivative of R with respect to x. Thus minimising $I \equiv \sum_i \int_{x_{i-1/2}}^{x_{i+1/2}} (d^3R/dx^3)^2 dx$, i.e. minimising the norm as in [16], is equivalent to minimising $I = \sum_i \int_{x_{i-1/2}}^{x_{i+1/2}} (d^2\rho_i/dx^2)^2 dx$. It can be verified that this is indeed true for the quartic spline defined herein. First note that

$$\begin{aligned} I &\equiv \sum_i \int_{x_{i-\frac{1}{2}}}^{x_{i+\frac{1}{2}}} \left[\frac{d^2\rho_i(x)}{dx^2}\right]^2 dx = \sum_i \frac{1}{h_i^3}\int_0^1 \left[\frac{d^2\rho_i(\xi)}{d\xi^2}\right]^2 d\xi = \sum_i \frac{1}{h_i^3}\int_0^1 \left[2a_i^{(2)} + 6a_i^{(3)}\xi + 12a_i^{(4)}\xi^2\right]^2 d\xi \\ &= \sum_i \frac{1}{h_i^3}\int_0^1 \left[\left(6\rho_{i+\frac{1}{2}} + 6\rho_{i-\frac{1}{2}} - \frac{7h_i^3}{20}M_{i-\frac{1}{2}} - \frac{3h_i^3}{20}M_{i+\frac{1}{2}} - 12\bar{\rho}_i\right) + 6h_i^3 M_{i-\frac{1}{2}}\xi + h_i^3\left(\frac{1}{2}M_{i+\frac{1}{2}} - \frac{1}{2}M_{i-\frac{1}{2}}\right)\xi^2\right]^2 d\xi, \end{aligned} \tag{43}$$

where (12)–(14) have been used to obtain the last line of (43). For a periodic domain, minimisation of (43) with respect to the coefficients $\rho_{i+1/2}$ and $M_{i+1/2}$, respectively, leads, after integration, to (20) and (21), respectively. These are the key conditions that turn the piecewise-quartic function into a quartic spline.

For a bounded domain, applying the same procedure to (43) for the coefficients $\rho_{5/2}, \rho_{7/2}, \ldots, \rho_{N-3/2}$ and $M_{5/2}, M_{7/2}, \ldots, M_{N-3/2}$ also leads to (24). Applying this procedure to (43) for $\rho_{1/2}$, $\rho_{3/2}$, $\rho_{N-1/2}$, $\rho_{N+1/2}$ and $M_{1/2}$, $M_{3/2}$, $M_{N-1/2}$, $M_{N+1/2}$, i.e. at the boundaries and at the first interior points, leads, for uniform resolution, to (28) and (29), (31)–(34) and (36) and (37), and also, for non-uniform resolution, to (63)–(70). These are exactly the results that are obtained if the definition of the quartic spline is closed by imposing the boundary conditions $d^2\rho/dx^2 = d^3\rho/dx^3 = 0$ at the endpoints $x_{1/2}$ and $x_{N+1/2}$. From (40), when constructing a quintic spline in terms of the cumulative mass function R, this corresponds to imposing $d^3R/dx^3 = d^4R/dx^4 = 0$ at the boundaries. These are the "natural" boundary conditions for a quintic spline [16], so $d^2\rho/dx^2 = d^3\rho/dx^3 = 0$ can be viewed as being the "natural" boundary conditions for the equivalent quartic spline defined herein.

A further property of classical quintic splines ([16], Section 5.5) is the "best approximation" property: of all interpolating piecewise-quintic functions, the quintic spline is optimal in the sense that it gives the smoothest such function to fit given data. In the present context, this means that the quartic spline defined herein can be viewed as having a "best approximation" property for the representation of the cumulative mass function R.

3. Monotonicity

Having determined the coefficients $\left(a_i^{(0)}, a_i^{(1)}, a_i^{(2)}, a_i^{(3)}, a_i^{(4)}\right)$ for each quartic $\rho_i(\xi)$, a monotonicity filter is used to optionally detect and correct spurious non-monotonic behaviour. The monotonicity algorithm follows the approach of [18,19] and has two parts: (i) detection of Control Volumes (CV's) where monotonicity is spuriously violated; and (ii) local modification of the quartic coefficients to achieve monotonicity within these flagged CVs.

There are two possible sources for the spurious violation of monotonicity: these can be characterised as being grid-scale and sub-grid-scale.

Firstly, the estimates $\{\rho_{i-1/2},\ i = 1, \ldots, N+1\}$ at the CV boundaries, as a complete set, are tested for undershoots and overshoots with respect to the given data $\{\bar{\rho}_i,\ i = 1, \ldots, N\}$. This is termed grid-scale violation and the algorithm in [18]

is used to modify the set $\{\rho_{i-1/2},\ i=1,\ldots,N+1\}$ to ensure that $\rho_{i-1/2}$ is within the range $[\bar{\rho}_{i-1},\bar{\rho}_i]$: if, initially, it is not, then it is minimally nudged to be so, i.e. $\rho_{i-1/2}\to\rho^*_{i-1/2}$, where $\rho^*_{i-1/2}=\bar{\rho}_{i-1}$ if $|\rho_{i-1/2}-\bar{\rho}_{i-1}|<|\rho_{i-1/2}-\bar{\rho}_i|$, and $\rho^*_{i-1/2}=\bar{\rho}_i$ if $|\rho_{i-1/2}-\bar{\rho}_{i-1}|>|\rho_{i-1/2}-\bar{\rho}_i|$.

Secondly, the local quartic may itself spuriously violate monotonicity within the interval over which it is defined. This is a sub-grid-scale violation and the algorithm proposed in [12] for a parabola is adapted to the quartic context, as follows.

3.1. Sub-grid-scale detection

Finding the roots of the cubic $d\rho_i(\xi)/d\xi=0$ to determine the number and locations of extrema is not straightforward. Therefore the sub-grid-scale detection algorithm instead uses the product of the slopes at both ends of the CV, i.e.

$$\mu_i\equiv(d\rho_i/d\xi)_{\xi=0}\times(d\rho_i/d\xi)_{\xi=1}=a_i^{(1)}\left(a_i^{(1)}+2a_i^{(2)}+3a_i^{(3)}+4a_i^{(4)}\right), \tag{44}$$

together with the properties of inflection points, to determine whether the quartic is monotone for $\xi\in[0,1]$. The two inflection points $\xi_i^{\pm}$, if they exist, are the roots of the quadratic equation $d^2\rho_i/d\xi^2\equiv 2a_i^{(2)}+6a_i^{(3)}\xi+12a_i^{(4)}\xi^2=0$ (i.e. $\xi_i^{\pm}=(-a_i^{(3)}\pm\sqrt{\omega_i})/(4a_i^{(4)})$, where $\omega_i\equiv(a_i^{(3)})^2-8a_i^{(2)}a_i^{(4)}/3\geqslant 0$ for inflection points to exist).

Let $s_i^{\pm}$ be the slopes at $\xi_i^{\pm}$ (i.e., $s_i^{\pm}\equiv(d\rho_i(\xi)/d\xi)_{\xi=\xi_i^{\pm}}$), let s_i^0 and s_i^1 be the slopes at $\xi=0$ and $\xi=1$, respectively (i.e., $s_i^0\equiv a_i^{(1)}$ and $s_i^1\equiv a_i^{(1)}+2a_i^{(2)}+3a_i^{(3)}+4a_i^{(4)}$), and define the marker v_i for the quartic $\rho_i(\xi)$ as

$$v_i=\begin{cases}0 & \text{if } \rho_i(\xi) \text{ is monotone for } \xi\in[0,1],\\ -1 & \text{if } \rho_i(\xi) \text{ has one minimum for } \xi\in[0,1],\\ +1 & \text{if } \rho_i(\xi) \text{ has one maximum for } \xi\in[0,1],\\ 2 & \text{if } \rho_i(\xi) \text{ has two extrema for } \xi\in[0,1]\\ 3 & \text{if } \rho_i(\xi) \text{ has three extrema for } \xi\in[0,1].\end{cases} \tag{45}$$

Depending on the sign of μ_i, there are three different cases to be considered.

3.1.1. $\mu_i<0$

Since the product μ_i of the end slopes is negative, there are either three extrema or there is a single extremum. Thus

$$v_i=\begin{cases}3 & \text{if } \omega_i\geqslant 0\oplus\xi_i^-(1-\xi_i^-)>0\oplus\xi_i^+(1-\xi_i^+)>0\oplus s_i^0s_i^-<0,\\ \operatorname{sign}(s_i^0) & \text{otherwise},\end{cases} \tag{46}$$

where $\operatorname{sign}(x\geqslant 0)\equiv 1$ and $\operatorname{sign}(x<0)\equiv -1$, and $\oplus$ denotes the logical "AND". [In (46): satisfaction of $\omega_i\geqslant 0$ ensures the existence of inflection points; satisfaction of $\xi_i^-(1-\xi_i^-)>0\oplus\xi_i^+(1-\xi_i^+)>0$ ensures that ξ_i^- and ξ_i^+ are both located within the interval $[0,1]$; $s_i^0s_i^-<0$ ensures that the product of the slope at the leftmost point of the interval with that at the leftmost point of inflection is negative; and $\operatorname{sign}(s_i^0)$ identifies whether a single extremum is a minimum or a maximum.]

3.1.2. $\mu_i>0$

Since the product μ_i of the end slopes is positive, there are either two or no extrema, i.e.

$$v_i=\begin{cases}2 & \text{if } \omega_i\geqslant 0\oplus\left\{\left[\xi_i^-(1-\xi_i^-)>0\oplus s_i^0s_i^-<0\right]\odot\left[\xi_i^+(1-\xi_i^+)>0\oplus s_i^0s_i^+<0\right]\right.\\ \qquad\left.\odot\left[\xi_i^-(1-\xi_i^-)>0\oplus\xi_i^+(1-\xi_i^+)>0\oplus s_i^-s_i^+<0\right]\right\},\\ 0 & \text{otherwise},\end{cases} \tag{47}$$

where $\odot$ denotes the logical "OR".

3.1.3. $\mu_i=0$

For this case either $s_i^0=0$ or/and $s_i^1=0$, and there are either two, one, or no extrema, i.e.

$$v_i=\begin{cases}2 & \text{if } \omega_i\geqslant 0\oplus\xi_i^-(1-\xi_i^-)>0\oplus\xi_i^+(1-\xi_i^+)>0\oplus\left(s_i^0s_i^-+s_i^1s_i^+\right)<0,\\ \operatorname{sign}(s_i^0-s_i^1) & \text{if } \omega_i\geqslant 0\oplus\left\{\left[\xi_i^-(1-\xi_i^-)>0\oplus\left(s_i^0+s_i^1\right)s_i^-<0\right]\odot\left[\xi_i^+(1-\xi_i^+)>0\oplus\left(s_i^0+s_i^1\right)s_i^+<0\right]\right\},\\ \operatorname{sign}(s_i^-) & \text{if } \omega_i\geqslant 0\oplus\xi_i^-(1-\xi_i^-)>0\oplus\xi_i^+(1-\xi_i^+)>0\oplus\left(s_i^0+s_i^1\right)=0,\\ 0 & \text{otherwise}.\end{cases} \tag{48}$$

Once values for the markers v_i have been assigned, all quartics with $v_i\neq 0$ are then modified, with one exception, which is now described.

3.2. Authenticity of a single extremum

When $v_i = \pm 1$, it is possible that the associated extremum is genuine and that it should not therefore be treated as being sub-grid-scale and spurious. Authenticity is determined by examination of various combinations of values at neighbouring points around the control-volume (i), as in [18]. In summary, when $v_i = \pm 1$, a quartic is judged to have spurious extrema if any of the following additional conditions hold:

$$\left.\begin{aligned}(\rho_{i-1/2}-\rho_{i-3/2})(\rho_{i+3/2}-\rho_{i+1/2}) &\geqslant 0\\ (\rho_{i-3/2}-\rho_{i-5/2})(\rho_{i-1/2}-\rho_{i-3/2}) &\leqslant 0\\ (\rho_{i+3/2}-\rho_{i+1/2})(\rho_{i+5/2}-\rho_{i+3/2}) &\leqslant 0\\ (\rho_{i-1/2}-\rho_{i-3/2})v_i &\leqslant 0\end{aligned}\right\}. \tag{49}$$

The extremum is otherwise considered to be genuine, consistent with the local distribution of gridpoint values, and the local quartic is then left unchanged and its associated v_i reset to zero.

3.3. Sub-grid-scale correction

Assume that an interval with index i has been detected that is not monotonic and in need of correction, i.e., $v_i \neq 0$. The underlying strategy adopted for imposing monotonicity is to: (i) always retain the conservation constraint; (ii) modify the quartic to be monotone within the interval [0,1]; and (iii) ensure that the modified quartic is bounded by its original endpoint values (i.e., $\rho_{i-1/2} \leqslant \rho_i(\xi) \leqslant \rho_{i+1/2}$). Depending upon the value of $\bar{\rho}_i$ within the range $[\rho_{i-1/2}, \rho_{i+1/2}]$ and, defining $\Delta\rho_i \equiv \rho_{i+1/2} - \rho_{i-1/2}$, there are five distinct regimes, plus an additional one when $\bar{\rho}_i$ is outside this range. It is straightforward to show that all sets of coefficients (50)–(54), given below, result in a $\rho_i(\xi)$ that locally satisfies the above three criteria for the range of $\bar{\rho}_i$ for which it is defined.

3.3.1. Regime 1: $\bar{\rho}_i \in \left[\rho_{i-1/2}, \rho_{i-1/2} + \frac{1}{5}\Delta\rho_i\right]$

Construct the monotonic quartic such that $\int_0^1 \rho_i(\xi)d\xi = \bar{\rho}_i,\ \rho_i(0) = \rho_{i-1/2},\ (d\rho_i/d\xi)|_{\xi=0} = (d^2\rho_i/d\xi^2)|_{\xi=0} = (d^3\rho_i/d\xi^3)|_{\xi=0} = 0$. Thus

$$a_i^{(0)} = \rho_{i-1/2}, \quad a_i^{(1)} = a_i^{(2)} = a_i^{(3)} = 0, \quad a_i^{(4)} = -5\rho_{i-1/2} + 5\bar{\rho}_i. \tag{50}$$

[Ideally one would like to impose $\rho_i(1) = \rho_{i+1/2}$, i.e. continuity of ρ at the other end of the interval, whilst dropping the condition $(d^3\rho_i/d\xi^3)|_{\xi=0} = 0$. This however fails to guarantee monotonicity.]

3.3.2. Regime 2: $\bar{\rho}_i \in \left[\rho_{i-1/2} + \frac{1}{5}\Delta\rho_i, \rho_{i-1/2} + \frac{2}{5}\Delta\rho_i\right]$

For this case it is possible to preserve continuity of ρ at both ends of the interval and to construct the monotonic quartic such that $\int_0^1 \rho_i(\xi)d\xi = \bar{\rho}_i,\ \rho_i(0) = \rho_{i-1/2}, \rho_i(1) = \rho_{i+1/2},\ (d\rho_i/d\xi)|_{\xi=0} = (d^2\rho_i/d\xi^2)|_{\xi=0} = 0$. Thus

$$a_i^{(0)} = \rho_{i-1/2}, \quad a_i^{(1)} = a_i^{(2)} = 0, \quad a_i^{(3)} = -16\rho_{i-1/2} - 4\rho_{i+1/2} + 20\bar{\rho}_i, \quad a_i^{(4)} = 15\rho_{i-1/2} + 5\rho_{i+1/2} - 20\bar{\rho}_i. \tag{51}$$

3.3.3. Regime 3: $\bar{\rho}_i \in \left[\rho_{i-1/2} + \frac{2}{5}\Delta\rho_i, \rho_{i-1/2} + \frac{3}{5}\Delta\rho_i\right]$

For this case it is possible to preserve continuity of ρ at both ends of the interval and to construct an antisymmetric (with respect to $\frac{1}{2}(\rho_{i-1/2} + \rho_{i+1/2})$) monotonic quartic such that $\int_0^1 \rho_i(\xi)d\xi = \bar{\rho}_i,\ \rho_i(0) = \rho_{i-1/2}, \rho_i(1) = \rho_{i+1/2},\ (d\rho_i/d\xi)|_{\xi=0} = (d\rho_i/d\xi)|_{\xi=1} = 0$. Thus

$$\begin{aligned}a_i^{(0)} &= \rho_{i-1/2}, \quad a_i^{(1)} = 0, \quad a_i^{(2)} = -18\rho_{i-1/2} - 12\rho_{i+1/2} + 30\bar{\rho}_i,\\ a_i^{(3)} &= 32\rho_{i-1/2} + 28\rho_{i+1/2} - 60\bar{\rho}_i, \quad a_i^{(4)} = -15\rho_{i-1/2} - 15\rho_{i+1/2} + 30\bar{\rho}_i.\end{aligned} \tag{52}$$

3.3.4. Regime 4: $\bar{\rho}_i \in \left[\rho_{i-1/2} + \frac{3}{5}\Delta\rho_i, \rho_{i-1/2} + \frac{4}{5}\Delta\rho_i\right]$

This is the antisymmetric image of regime 2 and obtained by fitting a quartic that satisfies: $\int_0^1 \rho_i(\xi)d\xi = \bar{\rho}_i,\ \rho_i(0) = \rho_{i-1/2}, \rho_i(1) = \rho_{i+1/2},\ (d\rho_i/d\xi)|_{\xi=1} = (d^2\rho_i/d\xi^2)|_{\xi=1} = 0$. Thus

$$\begin{aligned}a_i^{(0)} &= \rho_{i-1/2}, \quad a_i^{(1)} = -8\rho_{i-1/2} - 12\rho_{i+1/2} + 20\bar{\rho}_i, \quad a_i^{(2)} = 18\rho_{i-1/2} + 42\rho_{i+1/2} - 60\bar{\rho}_i,\\ a_i^{(3)} &= -16\rho_{i-1/2} - 44\rho_{i+1/2} + 60\bar{\rho}_i, \quad a_i^{(4)} = 5\rho_{i-1/2} + 15\rho_{i+1/2} - 20\bar{\rho}_i.\end{aligned} \tag{53}$$

3.3.5. Regime 5: $\bar{\rho}_i \in \left[\rho_{i-1/2} + \frac{4}{5}\Delta\rho_i, \rho_{i+1/2}\right]$

This is the antisymmetric image of regime 1 and obtained by fitting a quartic that satisfies: $\int_0^1 \rho_i(\xi)d\xi = \bar{\rho}_i,\ \rho_i(1) = \rho_{i+1/2},\ (d\rho_i/d\xi)|_{\xi=1} = (d^2\rho_i/d\xi^2)|_{\xi=1} = (d^3\rho_i/d\xi^3)|_{\xi=1} = 0$. Thus

$$a_i^{(0)} = -4\rho_{i+1/2} + 5\bar{\rho}_i, \quad a_i^{(1)} = 20\rho_{i+1/2} - 20\bar{\rho}_i, \quad a_i^{(2)} = -30\rho_{i+1/2} + 30\bar{\rho}_i,$$
$$a_i^{(3)} = 20\rho_{i+1/2} - 20\bar{\rho}_i, \quad a_i^{(4)} = -5\rho_{i+1/2} + 5\bar{\rho}_i. \tag{54}$$

3.3.6. Regime 6: $\bar{\rho}_i \notin [\rho_{i-1/2}, \rho_{i+1/2}]$

For the special case of $\bar{\rho}_i \notin [\rho_{i-1/2}, \rho_{i+1/2}]$ (i.e. $\bar{\rho}_i$ is outside the range of the left and right estimates $\rho_{i-1/2}$ and $\rho_{i+1/2}$), the only option left is to use a constant, i.e. $\rho_i(\xi) = \bar{\rho}_i$ and thus

$$a_i^{(0)} = \bar{\rho}_i, \quad a_i^{(1)} = a_i^{(2)} = a_i^{(3)} = a_i^{(4)} = 0. \tag{55}$$

Note that (50)–(54) are continuous across the four regime boundaries $\bar{\rho}_i = \rho_{i-1/2} + \frac{1}{5}\Delta\rho_i$, $\rho_{i-1/2} + \frac{2}{5}\Delta\rho_i$, $\rho_{i-1/2} + \frac{3}{5}\Delta\rho_i$, $\rho_{i-1/2} + \frac{4}{5}\Delta\rho_i$, i.e. the quartics in two adjacent regions degenerate to the same function at their common boundary. For example, the quartic defined by (52) for $\bar{\rho}_i = \rho_{i-1/2} + \frac{2}{5}\Delta\rho_i$ is identical to that defined by (51) for this value of $\bar{\rho}_i$.

4. Results

4.1. Preamble

See Table 1 for the nomenclature used within this section.

The test problems employed in [12] to illustrate the performance of PSM, with and without its monotonic filter, are also used herein to illustrate the performance of QSM, with and without its monotonic filter. In [12] PSM was compared with PPM [1] . Analogously, QSM is here compared with the Piecewise Quartic Method (PQM) with and without its filter [20]. The version of PQM used here is the method referred to in [20] as PQM ih_6/ih_5. It is the most accurate flavour amongst those presented in [20] and corresponds to an implicit reconstruction with sixth-order estimates for edge values and fifth-order ones for edge slopes. Performance is measured using the error measures suggested by [21] and summarised in Appendix B.

The computational domain used for the test problems is the interval $\Omega \equiv \{x \in [0, 2L] \equiv [x_{1/2}, x_{N+1/2}]\}$, which is divided into N sub-intervals $h_i \equiv x_{i+1/2} - x_{i-1/2}, i = 1, 2, \ldots, N$. Given the initial value problem of Section 2.1 with an average density distribution $(\bar{\rho}_1, \bar{\rho}_2, \ldots, \bar{\rho}_N)$, then the problem is to compute, using the QSM/PQM/PSM remapping algorithm, the discrete solution $(\bar{\rho}_1^{n+1}, \bar{\rho}_2^{n+1}, \ldots, \bar{\rho}_N^{n+1})$ at time $t^{n+1} \equiv t^n + \Delta t$ from the known solution at time t^n.

4.2. Uniform advection of a sine wave

This test is used to compare the performance of QSM against PSM for the infinitely differentiable distribution

$$\bar{\rho}(x, 0) = \sin\left(\frac{\pi x}{L}\right), \tag{56}$$

with $u(x, t) = U = 1$.

Table 2 displays the convergence of l_2 error for this test as a function of resolution N, when using PSM and QSM on a uniform grid (parameters as specified in the table and $h_i = h =$ constant). It can be verified from the data that PSM and QSM converge as $O(h^4)$ and $O(h^6)$, respectively, consistent with the properties of parabolic and quartic splines for sufficiently differentiable functions. [There is one, apparently anomalous result, inasmuch as l_2(QSM) with 512 points is not 64 ($\equiv 2^6$) times smaller than l_2(QSM) with 256 points, as one would expect, but only 10 times smaller. This is because the error with 512 points is at the limit of machine precision.] Furthermore the ratio r of the l_2 errors for PSM and QSM behaves as $O(h^{-2})$, as it should: even at the low resolution of 8 points, QSM has an l_2 error that is 50 times smaller than that for PSM, and the relative advantage increases dramatically as resolution is increased.

Table 1
Scheme acronyms.

Acronym	Scheme
PSM	Parabolic Spline Method [12]
PQM	Piecewise Quartic Method (ih_6/ih_5) [20]
QSM	Quartic Spline Method
PSM-M	Parabolic Spline Method with its Monotonic filter [12]
PQM-M	Piecewise Quartic Method with its Monotonic filter [20]
QSM-M	Quartic Spline Method with its Monotonic filter

Table 2
Convergence of l_2 error as a function of resolution N (=number of intervals) for uniform advection of a sine wave on a periodic domain with $L = 1/2,\ \varepsilon = 0.12$ ($\varepsilon = u\Delta t/h$ = Courant number) and 20 timesteps. The ratio r is defined as $r \equiv l_2(\text{PSM})/l_2(\text{QSM})$.

N	8	16	32	64	128	256	512
l_2(PSM)	0.549E−02	0.254E−03	0.143E−04	0.872E−06	0.541E−07	0.337E−08	0.211E−09
l_2(QSM)	0.109E−03	0.982E−06	0.120E−07	0.173E−09	0.264E−11	0.424E−13	0.440E−14
r	0.504E+02	0.258E+03	0.120E+04	0.504E+04	0.205E+05	0.796E+05	0.479E+05

4.3. Uniform advection of a generalised cosine-hill

Consider the generalised cosine-hill of order p, viz.

$$\bar{\rho}(x) = \begin{cases} \cos^p\left[\frac{\pi(x-L)}{2l}\right] & \text{for } L-l \leqslant x \leqslant L+l, \\ 0 & \text{otherwise}, \end{cases} \tag{57}$$

on the domain $[0, 2L]$ with p a positive integer and $0 < l < L$. This hill is continuous, has its first $p-1$ derivatives continuous, and its spectrum decays asymptotically as $k^{-(p+1)}$, where k is wavenumber.

Table 3 shows the performance of PSM and QSM for generalised cosine-hill with increasing degrees of smoothness p. As discussed in Section 3.2.3 of [12], the case $p = 4$ is the first for which the hill is sufficiently smooth to give errors that behave asymptotically as $O(h^4)$. Similarly, the case $p = 6$ for QSM is the first for which the hill is sufficiently smooth to give errors that behave asymptotically as $O(h^6)$.

For lower degrees of smoothness (i.e. $p = 2$ and $p = 4$), and consistent with the above discussion, it is seen from Table 3 that the ratio r of the l_2 errors for PSM and QSM does not behave asymptotically as $O(h^2)$ because the error is dominated by the discontinuities of low-order derivatives. In particular, for $p = 2,\ r$ remains almost unchanged as resolution is increased. However, for $p = 6$ and $p = 8,\ r$ increases significantly, and approximately as $O(h^2)$, as resolution is increased. [Note though, and similarly to the parenthetical comment in Section 4.2, this is not so for $N = 2048$ because the error with $N = 1024$ is already at almost machine precision and cannot be driven down much further.]

4.4. Uniform advection of an irregular signal

To test the monotonicity part of the algorithm, let the initial distribution be given by [18]:

$$\begin{aligned}\bar{\rho}(x,0;C) = {} & \{\tanh[c_1(x-c_2)] + \tanh[c_3(x-c_4)]\}\{1 + c_5\sin(2\pi c_6 x)\}\{1 + c_7\sin(2\pi c_8 x - c_9)\} \\ & + \{\tanh[c_{10}(x-c_{11})] + \tanh[-c_{10}(x-c_{12})]\} + c_{13},\end{aligned} \tag{58}$$

where $C = \{c_1, \ldots, c_{13}\}$ is a set of constants. Two variants of this problem are used for evaluation purposes: an irregular signal with mixed smooth and unsmooth parts, including quasi-discontinuities; and a profile having steep gradients.

The initial field $\bar{\rho}(x, 0; C_1)$ for uniform advection of an irregular signal is given (as in [18]) by (58), where $C_1 = [10, 0.3, -20, 0.6, 0.3, 11, 0.4., 10, 0.5, 200, .0.1, 0.3, 1]$, and it is advected with uniform velocity $U = 1$ on a uniform grid $\Delta x_i = \Delta x$ = constant, with $N = 50$ intervals, and $L = 1/2$. The timestep $\Delta t = 1/N_t$, where $N_t = 38$ is the number of timesteps per period, and the Courant number $\varepsilon \equiv U\Delta t/\Delta x \simeq 1.3$.

Table 4 displays the errors for PSM, PQM, QSM, PSM-M, PQM-M and QSM-M for this problem after one and five periods. It can be seen that overall QSM is more accurate than both PQM and PSM, even for a highly unsmooth and irregular profile. It can also be seen that, as expected theoretically, the accuracy of PQM lies between that of PSM and QSM. Furthermore, the high-order QSM monotonic filter maintains the advantage of QSM over PSM, especially around regions of steep gradients (e.g. the regions around $x = 0.1$ and $x = 0.6$). This is evident in Figs. 1 and 2 which graphically display the results of QSM and PSM summarised in Table 4. After one period (Fig. 1), it can be seen that both PSM-M and QSM-M selectively remove the undershoot that appears for x a little smaller than $x = 0.1$, and the overshoot for x a little larger, with negligible impact elsewhere. After five periods (Fig. 2), again both filters continue to be selectively activated for regions where needed whilst maintaining high-order accuracy elsewhere in the domain. Although the performance of PQM without its filter lies between PSM and QSM, PQM-M loses its advantage over PSM-M due its over-damping filter. This is clearly evident in Fig. 3 where there is good agreement between PQM and QSM (Fig. 3(a)), but PQM-M almost flattens the signal between $x = 0.4$ to

Table 3
Ratio $r \equiv l_2(\text{PSM})/l_2(\text{QSM})$ at different resolutions N for the generalised cosine-hill (57) with different powers p. $L = 1/2,\ l = 7/64,\ \varepsilon = 0.12$ and 20 time steps.

N	32	64	128	256	512	1024	2048
$p = 2$	0.174E+01	0.170E+01	0.166E+01	0.166E+01	0.165E+01	0.165E+01	0.165E+01
$p = 4$	0.360E+01	0.851E+01	0.102E+02	0.129E+02	0.176E+02	0.245E+02	0.344E+02
$p = 6$	0.213E+01	0.154E+02	0.891E+02	0.464E+03	0.216E+04	0.922E+04	0.143E+05
$p = 8$	0.165E+01	0.100E+02	0.653E+02	0.353E+03	0.165E+04	0.697E+04	0.202E+05

Table 4
Comparison of errors for uniform advection of an irregular signal for one and five periods with $N_t = 38$ timesteps per period and $\varepsilon \equiv U\Delta t/\Delta x \simeq 1.3$.

	l_1	l_2	l_∞	l_{min}	l_{max}
One period					
PSM	0.04124	0.06647	0.14795	−0.04899	−0.03574
PQM	0.03592	0.05487	0.11230	−0.08517	−0.00462
QSM	0.03356	0.05155	0.10361	−0.08189	−0.00860
PSM-M	0.03728	0.06853	0.14481	0.00000	−0.05400
PQM-M	0.04150	0.07442	0.14324	0.00000	−0.08189
QSM-M	0.02849	0.05635	0.12726	0.00000	−0.06194
Five periods					
PSM	0.05667	0.08835	0.18713	−0.05069	−0.03932
PQM	0.04269	0.06378	0.13722	−0.06100	−0.02569
QSM	0.04015	0.06128	0.12805	−0.05640	−0.02504
PSM-M	0.05370	0.08861	0.18226	0.00002	−0.05044
PQM-M	0.05351	0.08552	0.15286	0.00001	−0.10490
QSM-M	0.03577	0.06667	0.15026	0.00000	−0.06086

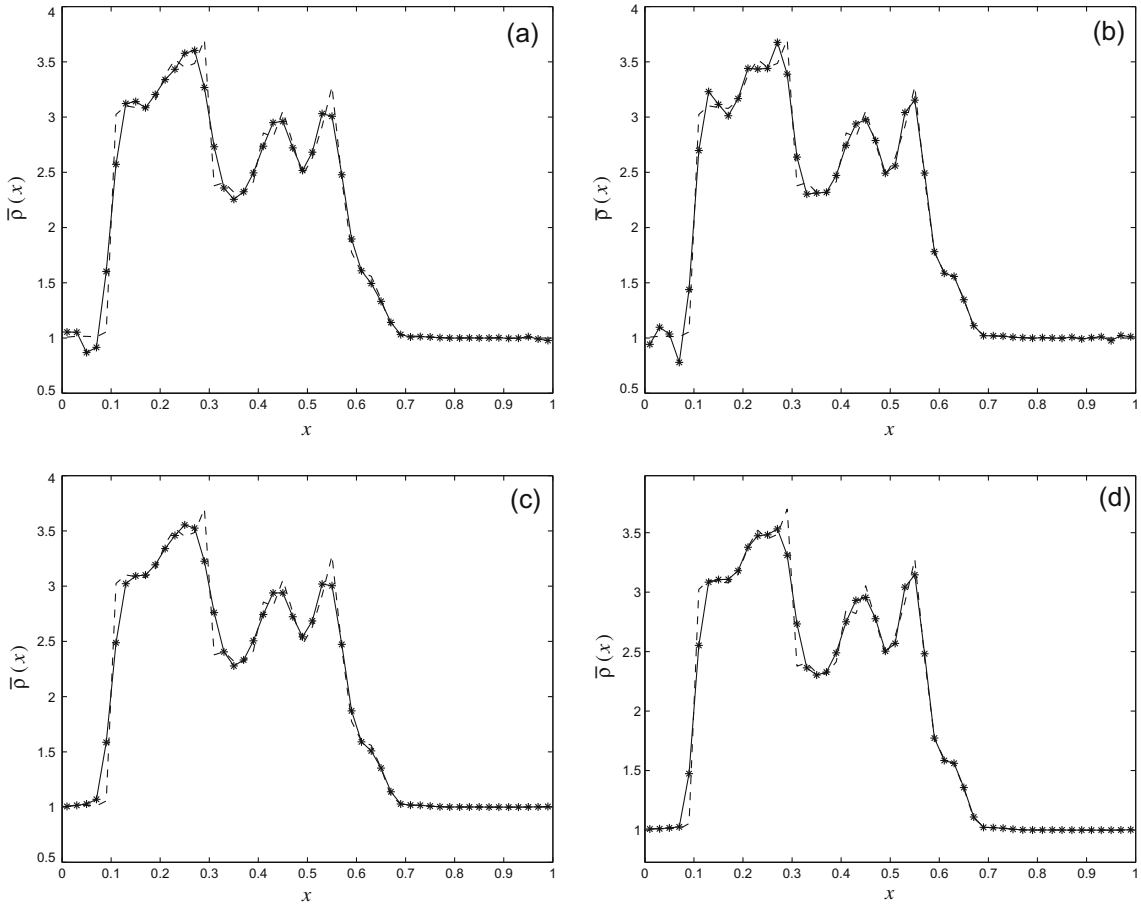

Fig. 1. Results after one complete period for the uniform advection of an irregular signal: (a) PSM; (b) QSM; (c) PSM-M; and (d) QSM-M. Parameters as in Table 4, and numerical solutions are shown with asterisks and continuous lines whilst analytical solutions are in dashed lines.

$x = 0.6$ in a similar manner to that observed for the PPM-filter [12,8]. A well known feature of the stringent PLM slope limiter (on which PQM-M is based) is that it causes a significant clipping but tends to preserve the sharpness of a step-like profile [8]. In contrast, the monotonic filter of QSM-M achieves monotonicity whilst maintaining close agreement with the analytical solution and without suffering from the excessive damping of PQM-M (Fig. 3(b)).

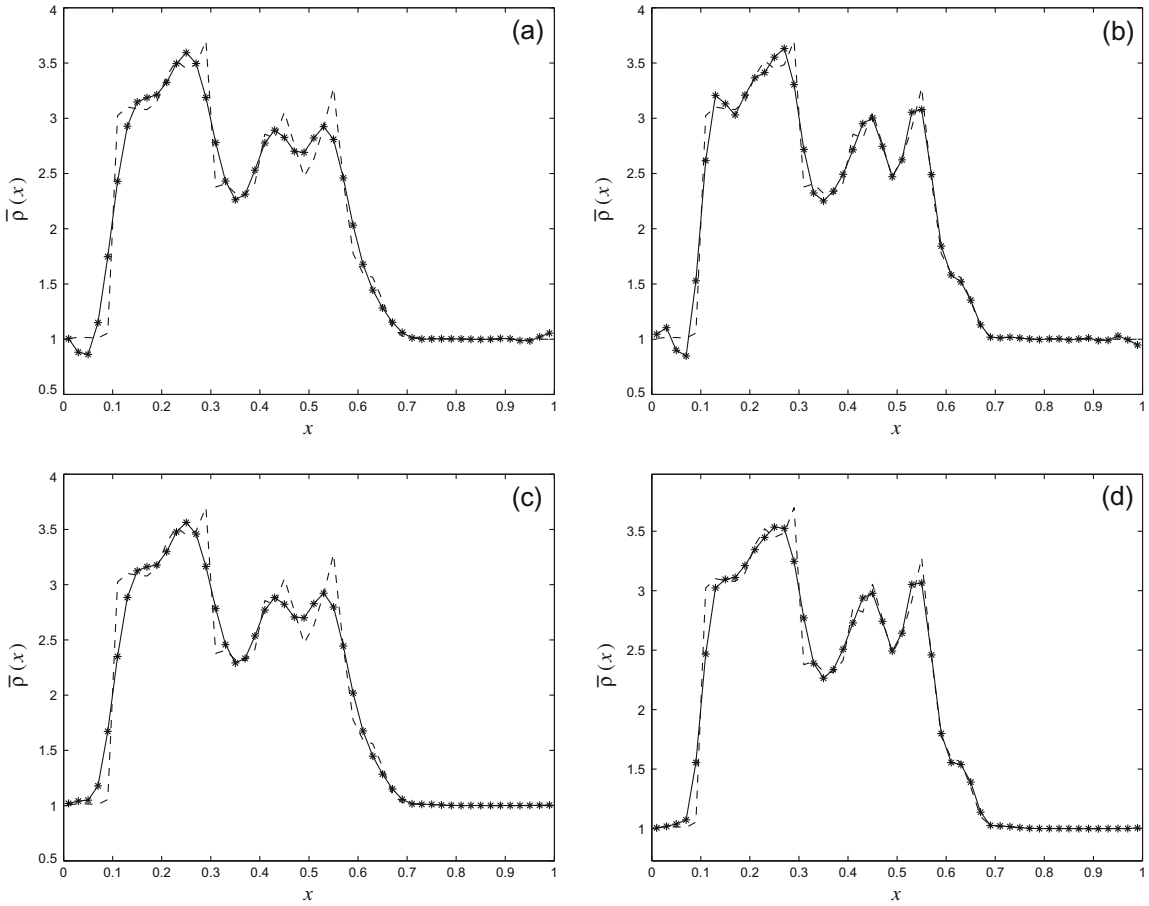

Fig. 2. As in Fig. 1 but for five periods: (a) PSM; (b) QSM; (c) PSM-M; and (d) QSM-M.

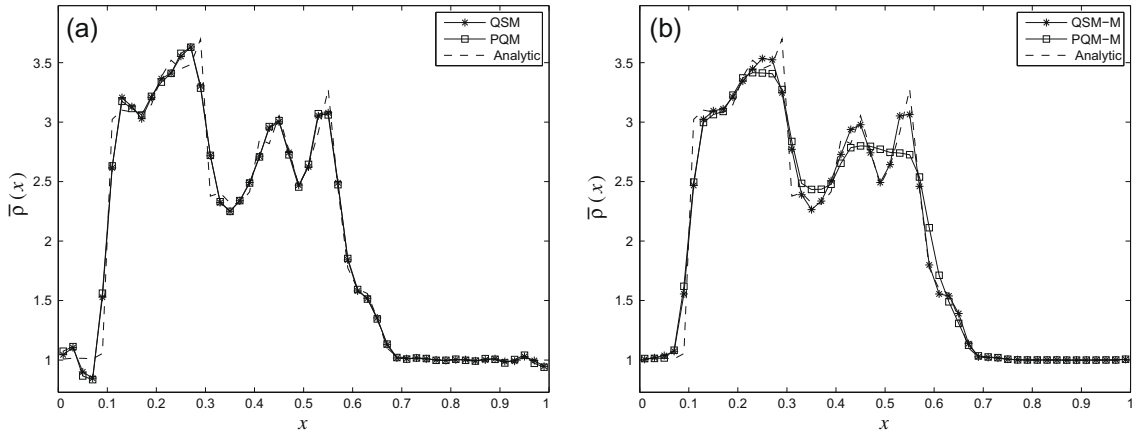

Fig. 3. Comparison of QSM and PQM for the advection of the irregular signal after five periods: (a) QSM vs PQM; (b) QSM-M vs PQM-M.

4.5. Uniform advection of a steep-gradient profile

The initial field $\bar{\rho}_0(x, 0; C_2)$ for uniform advection of a steep-gradient profile is given (as in [18]) by (58), where $C_2 = [200, 0.1, -200, 0.7, 0, 0, 0, 0, 0, 100, 0.3, 0.5, 0]$. It is advected using the same parameters as in the previous problem except that $N_t = 71$ and $\varepsilon \simeq 0.7$.

Table 5
Comparison of errors for uniform advection of a steep-gradient profile for one and five periods with $N_t = 71$ timesteps per period and $\varepsilon \equiv U\Delta t/\Delta x \simeq 0.7$.

	l_1	l_2	l_∞	l_{min}	l_{max}
One period					
PSM	0.06805	0.09068	0.14953	−0.04434	0.03617
PQM	0.06300	0.07090	0.11383	−0.05771	0.03552
QSM	0.05753	0.06641	0.10443	−0.05420	0.03177
PSM-M	0.05848	0.08961	0.14395	0.00000	−0.00022
PQM-M	0.04725	0.07783	0.13340	−0.00286	−0.00050
QSM-M	0.04319	0.07402	0.12305	0.00000	−0.00004
Five periods					
PSM	0.10491	0.11817	0.17850	−0.03928	0.03354
PQM	0.07734	0.08701	0.14119	−0.04999	0.04001
QSM	0.07178	0.08261	0.13159	−0.04150	0.03434
PSM-M	0.08825	0.11380	0.17285	0.00001	−0.00025
PQM-M	0.06275	0.09096	0.15700	−0.00150	−0.00251
QSM-M	0.05767	0.08591	0.14202	0.00000	−0.00016

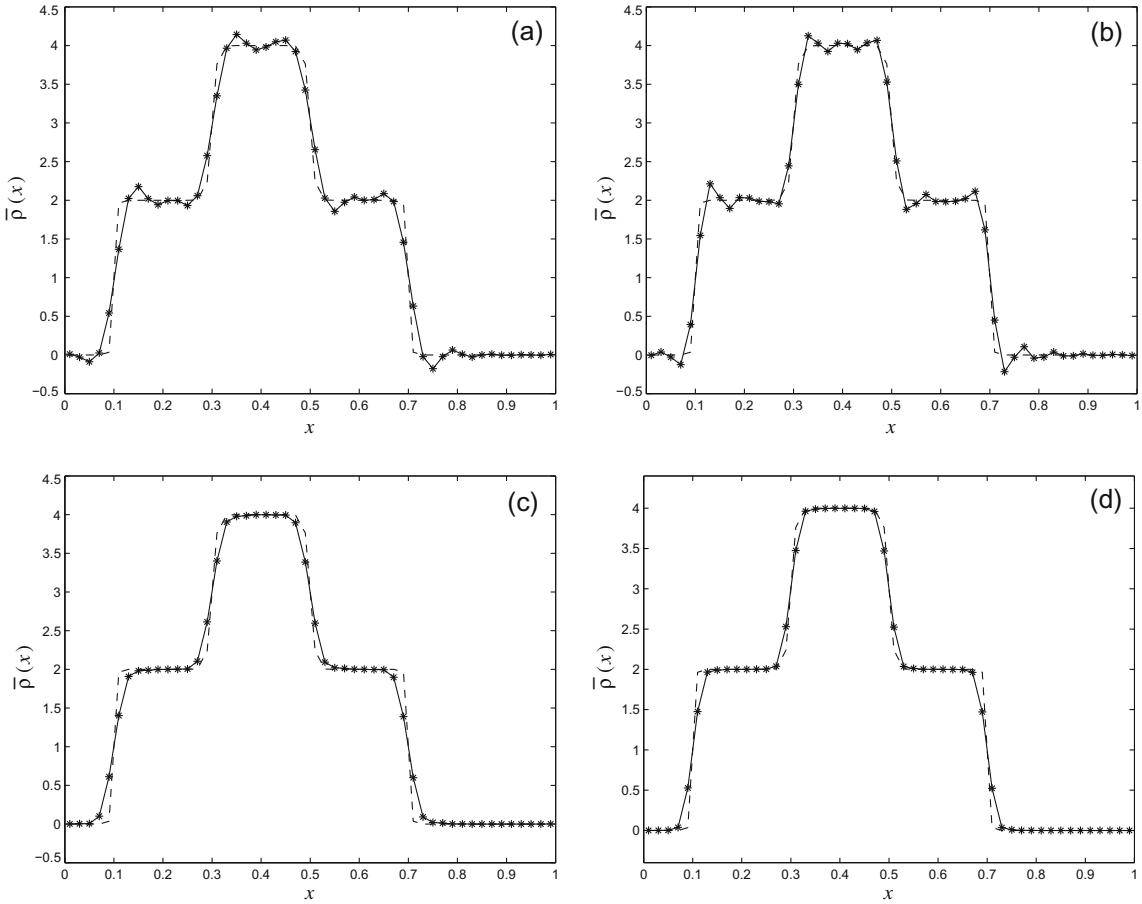

Fig. 4. As in Fig. 1 but for uniform advection of a steep-gradient profile with $\varepsilon \simeq 0.7$: (a) PSM, (b) QSM, (c) PSM-M; and (d) QSM-M.

Table 5 displays the errors for PSM, PQM, QSM, PSM-M, PQM-M and QSM-M for this problem. Similarly as for the previous problem, QSM is more accurate overall than both PSM and PQM, even for this problem which is an advection of a composition of quasi-step functions. Figs. 4 and 5 graphically display the results of QSM and PSM summarised in Table 5. It is seen that, as expected, both PSM-M and QSM-M filters behave very similarly but with QSM-M having sharper representations around regions of steep gradients: this is due to the use of a quartic spline rather than a parabolic one, together with a quartic

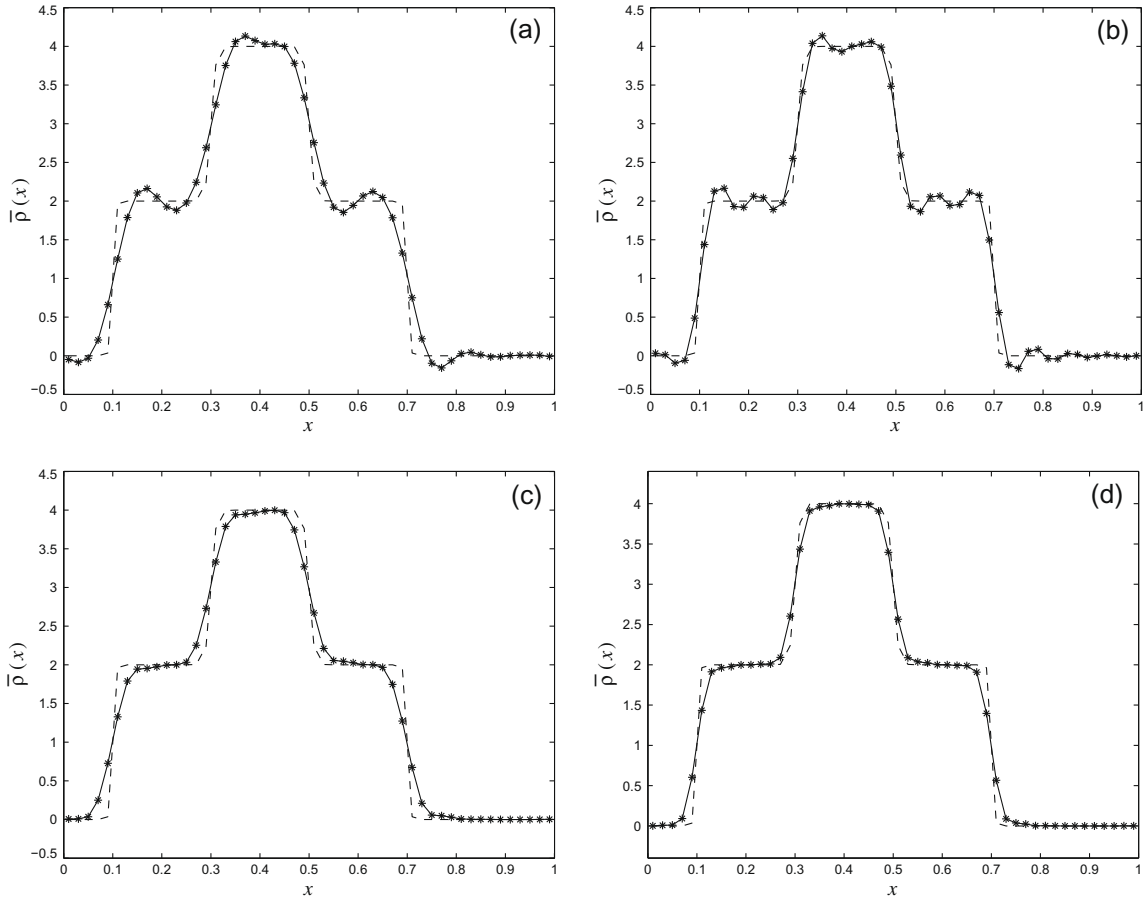

Fig. 5. As in Fig. 4 but for five periods: (a) PSM; (b) QSM; (c) PSM-M; and (d) QSM-M.

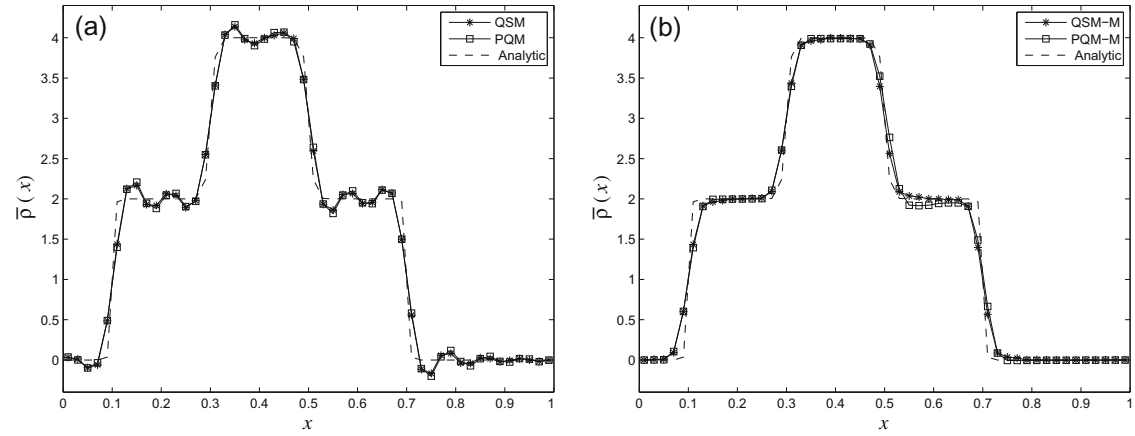

Fig. 6. Comparison of QSM and PQM for the advection of the steep gradient after five periods: (a) QSM vs PQM; (b) QSM-M vs PQM-M.

sub-grid-scale reconstruction even when the monotonic filter is activated. Unlike the irregular signal, for this problem (and for the reasons mentioned previously concerning the PLM/PQM slope limiter) PQM-M now maintains its advantage over PSM-M due to the quasi-step nature of the profile. This is also evident in Fig. 6 where there is a good visual agreement between QSM and PQM without and with their respective filters, albeit QSM-M is much sharper although the difference is less pronounced than for the irregular signal.

4.6. Computational cost

All the methods used here require a reconstruction and a common integration parts. For the reconstruction part, QSM requires the solution of one pentadiagonal system, whereas PQM solves two tridiagonal systems and PSM one tridiagonal system. The cost of a pentadiagonal system is approximately twice (although this can be only 9/5 using efficient algorithms as in [22]) that of a tridiagonal one and therefore, the computational cost of QSM is similar to that of PQM and twice that of PSM. This also agrees with run-times on a single processor for unoptimised codes (e.g. using the problem of the irregular signal after five periods, cpu-QSM = 1.1 cpu-PQM and 1.8 cpu-PSM). Note that the original QSM code was written for a general variable mesh, where the coefficients of the pentadiagonal matrix are long expressions (see Appendix A), whereas for simplicity, PQM was coded for a constant mesh, where the coefficient of the tridiagonal systems are simple numbers. For a general variable mesh, the implicit PQM would require the solutions of an extra 6×6 system of equations to compute the coefficients of every row of the two PQM diagonal matrices [20].

5. Conclusions

A quartic spline based remapping has been presented and tested for transport problems. Of all piecewise-quartic functions that satisfy the given mass (average density) distribution, it is an optimal reconstruction, since it possesses the *minimum norm* and *best approximation* properties [16].

A high-order monotonicity filter is also incorporated into the proposed scheme. It follows the same approach as in [12] by satisfying monotonicity whilst preserving mass and maintaining the highest order reconstruction possible. Results show that QSM with its filter is more selective and less damping than PSM and PQM with their respective filters: it removes spurious under/overshoots near discontinuities, with negligible impact on the smooth part of the solution. It is worth noting that this filter is independent of the underlying spline representation adopted here, and is of more general application.

For higher dimensional remappings, this 1D-algorithm can be combined with a splitting strategy. This can be a fixed-directional splitting (e.g. as in the Lin and Rood scheme with PPM [23]) or flow-dependent splitting such as the SLICE approach [2,3,13]. This makes possible a high-order accurate remapping for higher-dimensional problems without incurring a prohibitive computational cost, as demonstrated in [13] for the SLICE approach in both Cartesian and spherical geometries, and in [24] for remapping between spherical grids.

Acknowledgments

The authors thank the two referees for their helpful comments. The authors also wish to acknowledge Dr. Laurent White [20] for providing details of the implementation of PQM.

Appendix A. The non-uniform counterparts of (24), (25), and (28)–(37)

Following the four-step procedure outlined in Section 2.2, the non-uniform counterparts of (24) and (25) are found to be

$$\begin{aligned}
&\frac{h_{i-1}^3}{(h_{i-1}+h_i)(h_{i-1}+h_i+h_{i+1})}M_{i-\frac{3}{2}}\\
&+\left\{\left[4h_{i-1}+3h_i+\frac{h_{i-1}+h_i}{h_{i-1}}\left(\frac{h_ih_{i+1}}{h_i+h_{i+1}}+2h_i\right)\right]\frac{h_{i-1}}{h_{i-1}+h_i+h_{i+1}}+\frac{h_i^2(h_{i+1}+h_{i+2})}{(h_i+h_{i+1})(h_i+h_{i+1}+h_{i+2})}\right\}M_{i-\frac{1}{2}}\\
&+\left\{\left[\frac{h_{i-1}h_i}{h_{i-1}+h_i}+2h_i+\frac{h_{i-1}+h_i}{h_{i-1}}(3h_i+4h_{i+1})\right]\frac{h_{i-1}}{h_{i-1}+h_i+h_{i+1}}\right.\\
&\left.+\left[\frac{h_{i+1}h_{i+2}}{h_{i+1}+h_{i+2}}+2h_{i+1}+\frac{h_{i+1}+h_{i+2}}{h_{i+2}}(4h_i+3h_{i+1})\right]\frac{h_{i+2}}{h_i+h_{i+1}+h_{i+2}}\right\}M_{i+\frac{1}{2}}\\
&+\left\{\frac{(h_{i-1}+h_i)h_{i+1}^2}{(h_i+h_{i+1})(h_{i-1}+h_i+h_{i+1})}+\left[3h_{i+1}+4h_{i+2}+\frac{h_{i+1}+h_{i+2}}{h_{i+2}}\left(\frac{h_ih_{i+1}}{h_i+h_{i+1}}+2h_{i+1}\right)\right]\frac{h_{i+2}}{h_i+h_{i+1}+h_{i+2}}\right\}M_{i+\frac{3}{2}}\\
&+\frac{h_{i+2}^3}{(h_{i+1}+h_{i+2})(h_i+h_{i+1}+h_{i+2})}M_{i+\frac{5}{2}}=120(h_{i-1}+h_i+h_{i+1}+h_{i+2})R\left[x_{i-\frac{3}{2}},x_{i-\frac{1}{2}},x_{i+\frac{1}{2}},x_{i+\frac{3}{2}},x_{i+\frac{5}{2}}\right],
\end{aligned}\tag{59}$$

$$\begin{aligned}
\left[\frac{(h_{i-1}+h_i+h_{i+1})}{(h_{i-1}+h_i)h_{i+1}}+\frac{(h_i+h_{i+1}+h_{i+2})}{h_i(h_{i+1}+h_{i+2})}\right]\rho_{i+\frac{1}{2}}&=-\frac{h_i}{(h_{i-1}+h_i)^2}\bar{\rho}_{i-1}+\left[3-\frac{h_{i-1}(2h_{i-1}+3h_i)}{(h_{i-1}+h_i)^2}\right]\frac{1}{h_i}\bar{\rho}_i\\
&+\left[3-\frac{h_{i+2}(3h_{i+1}+2h_{i+2})}{(h_{i+1}+h_{i+2})^2}\right]\frac{1}{h_{i+1}}\bar{\rho}_{i+1}-\frac{h_{i+1}}{(h_{i+1}+h_{i+2})^2}\bar{\rho}_{i+2}\\
&-\frac{1}{120}\frac{h_{i-1}^3h_i}{(h_{i-1}+h_i)^2}M_{i-\frac{3}{2}}-\frac{h_i}{120}\left[\frac{h_{i-1}(4h_{i-1}+3h_i)}{(h_{i-1}+h_i)}+2h_i\right]M_{i-\frac{1}{2}}
\end{aligned}$$

$$+\frac{1}{120}\left\{h_{i+1}^2\left[3+\frac{h_{i+2}(2h_{i+1}+3h_{i+2})}{(h_{i+1}+h_{i+2})^2}\right]-h_i^2\left[3+\frac{h_{i-1}(3h_{i-1}+2h_i)}{(h_{i-1}+h_i)^2}\right]\right\}M_{i+\frac{1}{2}}$$
$$+\frac{h_{i+1}}{120}\left[2h_{i+1}+\frac{h_{i+2}(3h_{i+1}+4h_{i+2})}{(h_{i+1}+h_{i+2})}\right]M_{i+\frac{3}{2}}+\frac{1}{120}\frac{h_{i+1}h_{i+2}^3}{(h_{i+1}+h_{i+2})^2}M_{i+\frac{5}{2}}, \tag{60}$$

where $R\left[x_{i-\frac{3}{2}},x_{i-\frac{1}{2}},x_{i+\frac{1}{2}},x_{i+\frac{3}{2}},x_{i+\frac{5}{2}}\right]$ is obtained recursively from the Newton divided-difference formulae

$$R\left[x_{i-\frac{3}{2}},x_{i-\frac{1}{2}}\right]=\bar{\rho}_{i-1}, \tag{61}$$

$$R\left[x_{i-\frac{3}{2}},x_{i-\frac{1}{2}},\ldots,x_{i+j-\frac{1}{2}}\right]=\frac{R\left[x_{i-\frac{1}{2}},x_{i+\frac{1}{2}},\ldots,x_{i+j-\frac{1}{2}}\right]-R\left[x_{i-\frac{3}{2}},x_{i-\frac{1}{2}},\ldots,x_{i+j-\frac{3}{2}}\right]}{h_{i-1}+h_i+\cdots+h_{i+j-1}},\quad j=1,2,3. \tag{62}$$

Following the three-step procedure outlined in Section 2.3, the non-uniform counterparts of the remaining eight (near boundary) equations of (28)–(37) are found to be

$$M_{\frac{1}{2}}=0, \tag{63}$$

$$\frac{1}{120}\left[2h_1(3h_1+2h_2)+(h_2+h_3)(10h_1+7h_2)+\frac{h_2h_3(2h_2+3h_3)}{(h_2+h_3)}\right]M_{\frac{3}{2}}$$
$$+\frac{1}{120}\left[(3h_2+4h_3)h_3+3h_2(h_2+h_3)+\frac{h_1h_2^2}{(h_1+h_2)}\right]M_{\frac{5}{2}}+\frac{h_3^3}{120(h_2+h_3)}M_{\frac{7}{2}}=\frac{(\bar{\rho}_3-\bar{\rho}_2)}{(h_2+h_3)}-\frac{(\bar{\rho}_2-\bar{\rho}_1)}{(h_1+h_2)}, \tag{64}$$

$$\frac{h_{N-2}^3}{120(h_{N-2}+h_{N-1})}M_{N-\frac{5}{2}}+\frac{1}{120}\left[h_{N-2}(4h_{N-2}+3h_{N-1})+3h_{N-1}(h_{N-2}+h_{N-1})+\frac{h_{N-1}^2h_N}{(h_{N-1}+h_N)}\right]M_{N-\frac{3}{2}}$$
$$+\frac{1}{120}\left[\frac{(3h_{N-2}+2h_{N-1})h_{N-2}h_{N-1}}{(h_{N-2}+h_{N-1})}+2h_N(2h_{N-1}+3h_N)+(h_{N-2}+h_{N-1})(7h_{N-1}+10h_N)\right]M_{N-\frac{1}{2}}$$
$$=\frac{(\bar{\rho}_{N-1}-\bar{\rho}_{N-2})}{(h_{N-2}+h_{N-1})}-\frac{(\bar{\rho}_N-\bar{\rho}_{N-1})}{(h_{N-1}+h_N)}, \tag{65}$$

$$M_{N+\frac{1}{2}}=0, \tag{66}$$

$$\rho_{\frac{1}{2}}=\left[2-\frac{h_2}{(h_1+h_2)}\right]\bar{\rho}_1-\frac{h_1}{(h_1+h_2)}\bar{\rho}_2+\frac{h_1}{120}\left[3h_1^2+2h_2(3h_1+2h_2)\right]M_{\frac{3}{2}}+\frac{h_1h_2^3}{120(h_1+h_2)}M_{\frac{5}{2}}, \tag{67}$$

$$\rho_{\frac{3}{2}}=\frac{h_2}{(h_1+h_2)}\bar{\rho}_1+\frac{h_1}{(h_1+h_2)}\bar{\rho}_2-\frac{h_1h_2(3h_1+2h_2)}{60}M_{\frac{3}{2}}-\frac{h_1h_2^3}{120(h_1+h_2)}M_{\frac{5}{2}}, \tag{68}$$

$$\rho_{N-\frac{1}{2}}=\frac{h_{N-1}}{(h_{N-1}+h_N)}\bar{\rho}_N+\frac{h_N}{(h_{N-1}+h_N)}\bar{\rho}_{N-1}+\frac{h_{N-1}^3h_N}{120(h_{N-1}+h_N)}M_{N-\frac{3}{2}}+\frac{h_{N-1}h_N(2h_{N-1}+3h_N)}{60}M_{N-\frac{1}{2}}, \tag{69}$$

$$\rho_{N+\frac{1}{2}}=\left[2-\frac{h_{N-1}}{(h_{N-1}+h_N)}\right]\bar{\rho}_N-\frac{h_N}{(h_{N-1}+h_N)}\bar{\rho}_{N-1}-\frac{h_{N-1}^3h_N}{120(h_{N-1}+h_N)}M_{N-\frac{3}{2}}-\frac{h_N}{120}[2h_{N-1}(2h_{N-1}+3h_N)+3h_N^2]M_{N-\frac{1}{2}}. \tag{70}$$

Appendix B. Error measures

Performance is measured using the error measures suggested by [21], viz.

$$l_1\equiv\frac{I(|\bar{\rho}^{num}-\bar{\rho}^{an}|)}{I(|\bar{\rho}^{an}|)}, \tag{71}$$

$$l_2\equiv\frac{\sqrt{I(([\bar{\rho}^{num}-\bar{\rho}^{an}])^2)}}{\sqrt{I([\bar{\rho}^{an}]^2)}}, \tag{72}$$

$$l_\infty\equiv\frac{\max(|\bar{\rho}^{num}-\bar{\rho}^{an}|)}{\max(|\bar{\rho}^{an}|)}, \tag{73}$$

$$l_{min}\equiv\frac{\min(\bar{\rho}_{num})-\min(\bar{\rho}_{an})}{\max(\bar{\rho}_{an})-\min(\bar{\rho}_{an})}, \tag{74}$$

$$l_{max} \equiv \frac{\max(\bar{\rho}_{num}) - \max(\bar{\rho}_{an})}{\max(\bar{\rho}_{an}) - \min(\bar{\rho}_{an})}, \tag{75}$$

where $\bar{\rho}^{num}$ and $\bar{\rho}^{an}$ refer to the numerical and analytical solutions respectively, and $I(\bar{\rho})$ is a global integral (or global mass) given by

$$I(\bar{\rho}) \equiv \sum_{i=1}^{N} \bar{\rho}_i h_i \cong \int_0^{2L} \rho(x,t)\,dx. \tag{76}$$

References

[1] P. Colella, P. Woodward, The piecewise parabolic method (PPM) for gas-dynamical simulations, J. Comput. Phys. 54 (1984) 174–201.
[2] M. Zerroukat, N. Wood, A. Staniforth, SLICE: a semi-Lagrangian inherently conserving and efficient scheme for transport problems, Q. J. Roy. Meteorol. Soc. 128 (2002) 2801–2820.
[3] M. Zerroukat, N. Wood, A. Staniforth, SLICE-S: a semi-Lagrangian inherently conserving and efficient scheme for transport problems on the sphere, Q. J. Roy. Meteorol. Soc. 130 (2004) 2649–2664.
[4] M. Rančić, An efficient conservative monotonic remapping for semi-Lagrangian transport algorithms, Mon. Weather Rev. 123 (1995) 1213–1217.
[5] J.P.R. Laprise, A. Plante, A class of semi-Lagrangian integrated mass (SLIM) numerical transport algorithms, Mon. Weather Rev. 123 (1995) 553–565.
[6] B. Machenhauer, M. Olk, On the development of a cell-integrated semi-Lagrangian shallow water model on the sphere, in: ECMWF Workshop Proceedings: Semi-Lagrangian Methods, ECMWF, Reading, UK, 1996, pp. 213–228.
[7] B. Machenhauer, M. Olk, The implementation of the semi-implicit cell-integrated semi-Lagrangian models, Atmos.-Ocean 35 (1997) 103–126 (special issue).
[8] F. Xiao, T. Yabe, Completely conservative and oscillationless semi-Lagrangian schemes for advection transportation, J. Comput. Phys. 170 (2001) 498–522.
[9] R. Nair, B. Machenhauer, The mass conservative cell-integrated semi-Lagrangian advection scheme on the sphere, Mon. Weather Rev. 130 (2002) 649–667.
[10] R. Nair, J. Scroggs, F. Semazzi, Efficient conservative global transport schemes for climate and atmospheric chemistry models, Mon. Weather Rev. 130 (2002) 2059–2073.
[11] R. Nair, J. Scroggs, F. Semazzi, A forward trajectory global semi-Lagrangian transport scheme, J. Comput. Phys. 190 (2003) 275–294.
[12] M. Zerroukat, N. Wood, A. Staniforth, The Parabolic Spline Method (PSM) for conservative transport problems, Int. J. Numer. Meth. Fluid 11 (2006) 1297–1318.
[13] M. Zerroukat, N. Wood, A. Staniforth, Application of the Parabolic Spline Method (PSM) to a multi-dimensional conservative transport scheme (SLICE), J. Comput. Phys 225 (2007) 935–948.
[14] A. Staniforth, J. Côté, Semi-Lagrangian integration schemes for atmospheric models – a review, Mon. Weather Rev. 119 (1991) 2206–2223.
[15] B. van Leer, Towards the ultimate conservative difference scheme IV: a new approach to numerical convection, J. Comput. Phys. 23 (1977) 276–299.
[16] J.H. Ahlberg, E.N. Nilson, J.L. Walsh, The Theory of Splines and Their Applications, first ed., Academic Press, London, 1967.
[17] W. Press, S. Teukolsky, W. Vetterling, B. Flannery, Numerical Recipes in FORTRAN: The Art of Scientific Computing, second ed., Cambridge University Press, Cambridge, UK, 1992.
[18] M. Zerroukat, N. Wood, A. Staniforth, A monotonic and positive-definite filter for a Semi-Lagrangian Inherently Conserving and Efficient (SLICE) scheme, Q. J. Roy. Meteorol. Soc. 131 (2005) 2923–2936.
[19] M. Zerroukat, N. Wood, A. Staniforth, Erratum for: a monotonic and positive-definite filter for a Semi-Lagrangian Inherently Conserving and Efficient (SLICE) scheme, Q. J. Roy. Meteorol. Soc. 131, 2923–2936, Q. J. Roy. Meteorol. Soc. 134 (2008) 280.
[20] L. White, A. Adcroft, A high-order finite volume remapping scheme for nonuniform grids: the piecewise quartic method (PQM), J. Comput. Phys. 227 (2008) 7394–7422.
[21] D.L. Williamson, J.B. Drake, J.J. Hack, R. Jakob, P.N. Swarztrauber, A standard test set for numerical approximations to the shallow-water equations in spherical geometry, J. Comput. Phys. 102 (1992) 211–224.
[22] A.D.A. Hadj, M. Elouafi, A fast numerical algorithm for the inverse of a tridiagonal and pentadiagonal matrix, Appl. Math. Comput. 202 (2008) 441–445.
[23] S.J. Lin, R.B. Rood, Multidimensional flux-form semi-Lagrangian transport schemes, Mon. Weather Rev. 124 (1996) 2046–2070.
[24] P.H. Lauritzen, R.D. Nair, Monotone and conservative cascade remapping between spherical grids (CaRS): regular latitude-longitude and cubed-sphere grids, Mon. Weather Rev. 136 (2008) 1416–1432.